PERGAMON

Journal of the Mechanics and Physics of Solids
47 (1999) 785–815

JOURNAL OF THE
MECHANICS AND
PHYSICS OF SOLIDS

The viscoplastic compaction of composite powders

B. Storåkers[a,*], N.A. Fleck[b], R.M. McMeeking[c]

[a] *Department of Solid Mechanics, Royal Institute of Technology, Stockholm, Sweden*
[b] *Cambridge University Engineering Department, Trumpington Street, Cambridge CB2 1PZ, U.K.*
[c] *Department of Mechanical and Environmental Engineering, University of California, Santa Barbara, California 93106, U.S.A.*

Received 12 January 1998; in revised form 29 May 1998

Abstract

A model for the densification of spherical powders is developed for the early stages of cold and hot compaction under general loading. General viscoplastic properties are adopted which reduce to strain hardening plasticity at ambient temperature and to power law creep at elevated temperature. A large strain analysis is carried out to determine the macroscopic compaction behaviour, based on the affine motion of particles with viscoplastic dissipation occurring at the contacts between particles. Random packing is assumed and the model includes the increase in the number of contacts per particle with densification. A general prescription is given for computing the macroscopic stress as a function of strain rate and accumulated strain. Detailed results are presented for yield surfaces and creep dissipation surfaces after isostatic and closed die compaction. A scalar constraint factor is derived for a random mixture of two populations of particles with different sizes and strengths. The predictions include the limiting case of deformable spheres reinforced with rigid spheres of different size.

Keywords: Indentation and hardness; Powder compaction; Anisotropic material; Constitutive behaviour; Porous material

1. Introduction

The compaction of powders to form both bulk materials and net-shaped parts has become a successful and well-established process for metals, alloys, polymers and

* Corresponding author. Tel.: (46) 8 790 8641. Fax: (46) 8 411 2418. E-mail: bertil@hallf.kth.se

0022–5096/99/$ - see front matter
PII: S0022–5096(98)00076–3

ceramics. In the powder metallurgy (PM) industry a popular process route is cold compaction by rate-independent plasticity, followed by pressureless sintering by diffusional flow. In hot pressing, compaction is by power law creep and/or diffusional flow. Although significant empirical progress has been made to optimise compaction procedures with respect to pressure, temperature and time, a concise and general micromechanical model, free from phenomenological assumptions, has been lacking. Early constitutive descriptions have been empirical in nature, with no underlying modelling (see for example, Kuhn and Downey, 1971; Shima and Oyane, 1976). Herein, a micromechanical model is developed for powder compaction by both plasticity and power-law creep, with the relative density in the practical range of 0.6–0.8. The essential physics are the relationship between the macroscopic strain and the local kinematics of particle contact, and the relationship between local contact loads and the resulting macroscopic stress. The model is appropriate for the so-called Stage I regime, with relative density of the compact approximately in the range 0.6–0.8.

Substantial progress has already been made in the modelling of the plastic and creep responses of powder aggregates. Wilkinson and Ashby (1975) laid the foundations for isostatic compaction by power law creep, and Fischmeister and co-workers (Fischmeister et al., 1978; Fischmeister and Arzt, 1983) addressed the parallel problem of isostatic compaction by plastic flow. Several elements from these studies were combined by Helle et al. (1985). For the early state (designated Stage I), when particulate topology with interconnected porosity still prevails, they used the geometric model of Arzt (1982) to predict the area and number of contacts during deformation. Elementary models for the generation of interparticle loads were used to predict the plastic and the creep response of the aggregate. These ideas were extended to non-isostatic deformation rates for rate-independent plasticity (Fleck et al., 1992a), for power law creep (Kuhn and McMeeking, 1992; Fleck et al., 1992b) and for sintering (Jagota et al., 1988; Jagota et al., 1990). The effect of previous anisotropic straining of the powders, which determines the contact area distribution in particles, was introduced by Jagota et al. (1988) and by Fleck (1995). Fleck (1995) also explored the effects upon the yield surface of the shear strength and cohesive strength of the contacts.

To date, most theoretical studies have focused on the compaction of monolithic equi-sized spherical powder; the next step is to address the more practical problem of the compaction of a powder composite, comprising two populations of particles of unequal size and strength. Recently, new theoretical tools have become available for analysing the compaction of such a composite powder, and it is timely to synthesise a powder compaction model combining these fresh results with some robust elements of the previous work.

One of the new tools is a generic treatment of the mutual indentation of two viscoplastic spheres of dissimilar diameter and strength (Storåkers et al., 1997; Storåkers, 1997). This advance builds on the analysis of spherical (Brinell) indentation of a power law deformation theory solid by Hill et al. (1989). The relation between indentation depth and contact area was found to be geometrically invariant and from a detailed finite element study, the compliance properties for two equally sized spheres was calculated. Explicit results in this spirit have subsequently been computed for

creep (Bower et al., 1993; Storåkers and Larsson, 1994), for plastic flow theory (Biwa and Storåkers, 1995; Ogbonna et al., 1995) and for viscoplasticity (Ogbonna et al., 1995; Storåkers et al., 1997). From this standpoint, isostatic cold and hot compaction was recently analysed by Larsson et al. (1996); the model compared favourably with earlier experimental observations for Stage I compaction of copper, tin, bitumen and lead. One of the present objectives is to generalise this strategy to account for non-isostatic cases.

An additional tool for the construction of a compaction model for powder composites is a knowledge of the neighbour statistics for a mixture of spherical particles made from two different materials and two different sizes, as provided by Turner and Ashby (1995a, b).

Robust elements from previous work include the cumulative radial distribution function for particle neighbour positions in a monodispersed powder and the associated change in the number of contacts during straining (Arzt, 1982), the concept of affine deformations for particle aggregates (Fleck et al., 1992a) and the generation of anisotropic distributions of contact area and contact load due to arbitrary deformations (Fleck, 1995). Fleck (1995) found that the plastic dissipation due to tangential loads is a small fraction of the total for general straining of a rigid, ideally plastic compact. We shall take advantage of this to make the important simplifying assumption of frictionless indentation between particles.

It is the present purpose to derive general macroscopic constitutive equations for the compaction of homogeneous and composite powders. To begin, the kinematics associated with affine motion are outlined, viscoplastic indentation theory is reviewed and the macroscopic stress is related to the local contact forces between individual particles. Compaction relations are then obtained for a random homogeneous aggregate of identical spheres. The full macroscopic theory, with all parameters having a physical interpretation, are specified and the resulting densification equations are given for practical cases. For both isostatic and closed die compaction, the evolution of the yield surface is calculated for rate independent plasticity, and creep dissipation surfaces are determined for power law creep. The results are generalised for a composite powder comprising a random mixture of two populations of spheres. A constraint factor to account for reinforcement by particles of dissimilar strength and size is proposed. Finally, the domain of validity of the model is discussed.

2. Foundations of the compaction model

2.1. *Kinematics*

Consider a powder aggregate consisting of spherical particles of two different radii R_1 and R_2, in a state of dense random packing as shown in Fig. 1. Following a standard procedure for granular materials, e.g. Christoffersen et al. (1981) and Walton (1987), affine deformations are assumed such that each particle translates at the velocity prescribed for its centre. Where contact is made between neighbours, isolated indentations can occur. The aggregate is assumed to experience a macroscopically

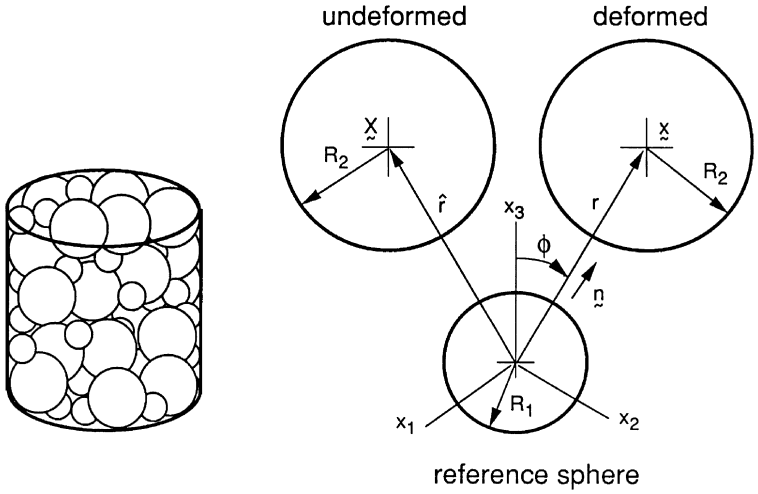

Fig. 1. A dense random packing of spheres of two different radii, and the relative motion of two adjacent particles.

homogeneous deformation which therefore prescribes the motion of the particles' centres. Placing the stationary origin at the centre of a reference particle as shown in Fig. 1, we see that a given particle with its centre initially at position $\mathbf{X}$ (a distance $\hat{r}$ from the reference particle) is carried to a new location with its centre at position

$$\mathbf{x} = \mathbf{F} \cdot \mathbf{X} \tag{1}$$

where $\mathbf{F}$ is the macroscopic deformation gradient. It is convenient to decompose $\mathbf{x}$ into its magnitude r, designating the current distance from the reference particle centre to the centre of the particle of interest, and the unit vector $\mathbf{n}$, defining the orientation with respect to the reference particle, as shown in Fig. 1. Then,

$$\mathbf{x} = r\mathbf{n} \tag{2}$$

Based on the macroscopic deformation gradient, the stretch ratio λ can be computed as

$$\lambda(\mathbf{n}) = \frac{r}{\hat{r}} = [\mathbf{n} \cdot (\mathbf{F}^{-1})^{\mathrm{T}} \cdot \mathbf{F}^{-1} \cdot \mathbf{n}]^{-1/2} \tag{3}$$

If the two particles are close enough, they will indent each other as shown in Fig. 2. The overlap of particle centres h, a function of $\mathbf{n}$, serves as a useful indentation parameter and is given by

$$h(\mathbf{n}) = R_1 + R_2 - r(\mathbf{n}) = R_1 + R_2 - \lambda(\mathbf{n})\hat{r} \tag{4}$$

where R_1 and R_2 are the radii of the particles indenting each other. Note that h is positive for those pairs of particles which flatten each other in compression. The rate of indentation is given by

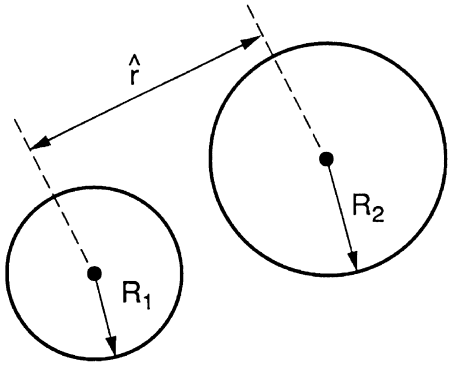

(a) Undeformed State

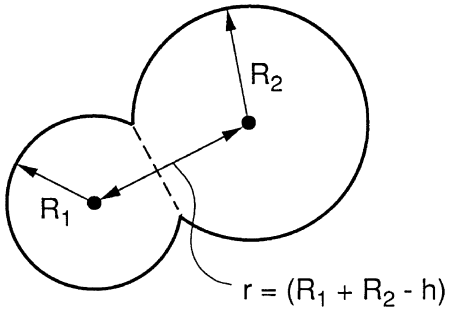

(b) Currently Indented at Stretch Ratio $\lambda = r/\hat{r}$

Fig. 2. Two nearby particles which eventually touch and indent each other.

$$\dot{h} = -\dot{\lambda}\hat{r} \tag{5}$$

and $\dot{\lambda}$ is related to the macroscopic deformation rate **D** by

$$\dot{\lambda} = \lambda n_i D_{ik} n_k \tag{6}$$

2.2. *Viscoplastic indentation*

Consider two spherical particles experiencing monotonic mutual indentation as shown in Fig. 3. The two spheres are labelled 1 and 2, with radii R_1 and R_2, respectively. In the current state the contact area is of radius a and the particle centres have overlapped by h. Particle 1 is made from viscoplastic material with a uniaxial stress response given by

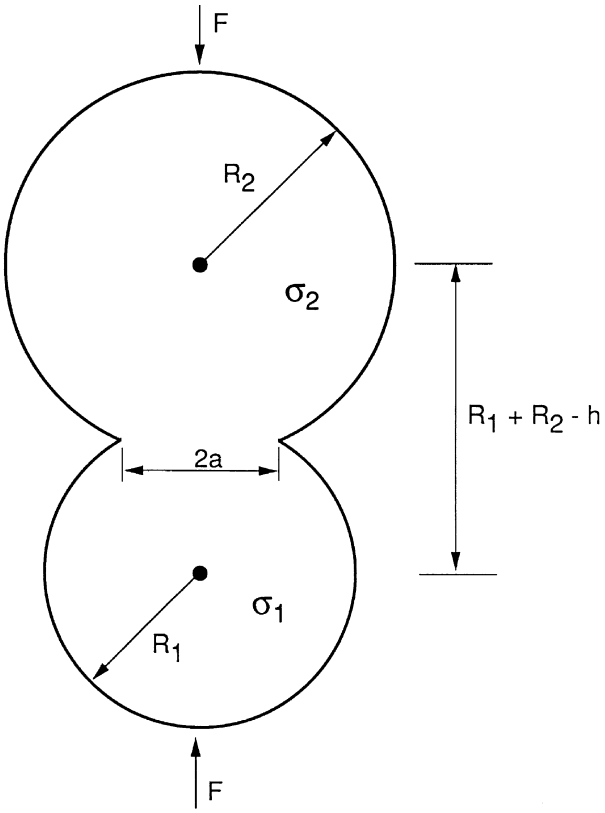

Fig. 3. Two particles identing each other.

$$\sigma = \sigma_1 \varepsilon^M \dot{\varepsilon}^N \tag{7}$$

where σ_1 is a strength parameter, ε is the axial strain, $\dot{\varepsilon}$ is its rate, M is a hardening exponent and N is a creep index. An equivalent law governs material 2, with σ_1 replaced by σ_2. Both particles are taken to have the same hardening exponents and the same creep indices. Based on indentation theory and von Mises isotropic flow theory, the solution for the indentation load F is (Storåkers et al., 1997; Storåkers, 1997)

$$F = \eta h^{(2+M-N)/2} \dot{h}^N \tag{8}$$

where

$$\eta = 2^{1-\frac{M}{2}-\frac{3N}{2}} 3^{1-M-N} (1+2N) \pi c^{2+M+N} \sigma_0 {R_0}^{1-\frac{M}{2}-\frac{N}{2}} \tag{9}$$

$$R_0^{-1} = R_1^{-1} + R_2^{-1} \tag{10}$$

$$\sigma_0^{-q} = \sigma_1^{-q} + \sigma_2^{-q} \tag{11}$$

and

$$q = (M+N)^{-1} \tag{12}$$

The parameter c in eqn (9) is an indentation invariant, and depends only upon the material constants M and N. From a detailed finite element study it was found that the invariant c is given, to within a very good approximation, by

$$c^2 = 1.43 \exp\left[-0.97(M+N)\right] \tag{13}$$

The contact radius a is related to the indentation depth h by

$$a^2 = 2c^2 h R_0 \tag{14}$$

For later use it is helpful to introduce a creep potential $\phi_c(\dot{h})$ for a single contact by integrating the indentation load F with respect to $\dot{h}$ at fixed h, so that

$$\phi_c(\dot{h}) \equiv \int_0^{\dot{h}} F(\dot{h}')\, \mathrm{d}\dot{h}' \Leftrightarrow F = \partial\phi_c/\partial\dot{h} \tag{15}$$

giving, via eqn (8),

$$\phi_c = \frac{1}{N+1} \eta h^{\frac{2+M-N}{2}} \dot{h}^{N+1} \tag{16}$$

2.3. *Macroscopic stress*

In the early stages of compaction, when particles can still be represented as spheres with only small circular contacts around their surface (i.e. Stage I), a macroscopic viscoplastic potential $\Phi(\mathbf{D})$ can be computed as

$$\Phi = V^{-1} \sum_J \{\phi_c\}_J \tag{17}$$

where V is a representative volume of the powder aggregate containing many particles, the summation is carried out over all particle–particle junctions in the aggregate and $\{\phi_c\}_J$ is the value of the potential from eqn (16) for junction J. This formulation neglects the dissipation due to shearing motions at each junction and is exact for frictionless spheres. Our experience (Kuhn and McMeeking, 1992; Fleck 1995) suggests that for values of q greater than about two, the dissipation due to shearing motions can be neglected in the macroscopic average even for well-bonded aggregates.

The macroscopic average stress $\mathbf{\Sigma}$ for the aggregate subjected to a deformation rate $\mathbf{D}$ is then given by

$$\Sigma_{ik} = \frac{\partial\Phi}{\partial D_{ik}} = V^{-1} \sum_J \left\{ F \frac{\partial\dot{h}}{\partial D_{ik}} \right\}_J \tag{18}$$

where $F(\dot{h})$ is given by eqn (8). In the case of a cohesionless powder F vanishes when

the particles lose contact at a junction. In principle, eqn (18) gives the exact result if $\dot{h}$ were known at each junction. Instead, we assume affine deformation, in which $\dot{h}$ is given by eqns (5) and (6). The macroscopic stress is then given by

$$\Sigma_{ik} = -\frac{1}{V}\sum_{J}\{F\lambda\hat{r}n_i n_k\}_J \tag{19}$$

This result is equivalent to an average for the aggregate value given by Christoffersen et al. (1981).

In the following section, Stage I compaction of a homogeneous viscoplastic aggregate is addressed. Then, the analysis is broadened to the case of composite powders.

3. Homogeneous aggregate

Consider first an aggregate of n uniform spheres of radius R_1 all made from the same material 1 with strength parameter σ_1. The aggregate volume V is related to the volume of each sphere V_1 and to the relative density D by

$$V = \frac{V_1 n}{D} = \frac{4\pi R_1^3 n}{3D} \tag{20}$$

The initial relative density is taken to be that of dense random packing, $D_0 = 0.64$. From a distribution function obtained by Mason (1968), based on data by Scott (1962), Arzt (1982) proposed that this initial state could be approximated by a cumulative radial distribution function for particle centres adjacent to a reference sphere:

$$G(\hat{r}) = Z_0 + C\left(\frac{\hat{r}}{2R_1} - 1\right), \quad \frac{\hat{r}}{2R_1} \geqslant 1 \tag{21}$$

where G is the number of particle centres within a radius $\hat{r}$ from the centre of the reference particle and Z_0 and C are constants. (This form is sufficient for the values of $\hat{r}/R_1$ which we encounter in our model.) The best estimates for the constants are $C = 15.5$ and $Z_0 = 7.3$ (Arzt, 1982). The latter value implies that on average each sphere initially has 7.3 contacts with neighbours.

For affine deformations, eqn (4) provides the indentation h for two particles originally having their centres a distance $\hat{r}$ apart. Furthermore, with $S_1 = 4\pi R_1^2$, eqn (21) shows that there are initially $\mathrm{d}G/S_1$ particles per unit reference sphere surface area having their centres between $\hat{r}$ and $(\hat{r}+\mathrm{d}\hat{r})$ from the reference particle. Summing over all such contacts and attributing half of the contribution to each particle making the contact, we find that the contribution to eqn (19) from a typical reference particle is

$$\Sigma_{ik} = -\frac{R_1 Z_0}{VS_1}\int_{S_1}\mathrm{d}S_1[F_1\lambda n_i n_k] - \frac{1}{2VS_1}\int_{S_1}\mathrm{d}S_1[\lambda n_i n_k]\int_{2R_1}^{2R_1/\lambda}\mathrm{d}\hat{r}\left[F\hat{r}\frac{\mathrm{d}G}{\mathrm{d}\hat{r}}\right] \tag{22}$$

where F_1 is the load on an original contact, of orientation $\mathbf{n}$, which has existed from

the beginning of consolidation and therefore for which $\hat{r} = 2R_1$. For these original contacts, F_I follows from eqn (8) as

$$F_I = \eta h_I^{\frac{2+M-N}{2}} \dot{h}_I^N \tag{23}$$

expressed in terms of the overlap h_I,

$$h_I \equiv 2R_1[1-\lambda(\mathbf{n})] \tag{24}$$

and the rate of overlap

$$\dot{h}_I = -2R_1\dot{\lambda}(\mathbf{n}) \tag{25}$$

by eqns (4) and (5), respectively.

The integrals with respect to S_1 in eqn (22) are taken over the surface of the reference particle with radius R_1. The first term on the right hand side of eqn (22) is the contribution from these original contacts whereas the second term arises from contacts made during compaction. Such new contacts are associated with particles originally having their centres beyond a distance $2R_1$ from the reference particle centre but not beyond a distance $2R_1/\lambda$ from it. Since there are n particles within the aggregate volume V, the total stress $\mathbf{\Sigma}$ is simply n times the result given in eqn (22).

It follows from eqns (4), (5), (8) and (23) that the load F on a new contact can be expressed in terms of F_I as

$$F = \left(\frac{1-\lambda\hat{r}/2R_1}{1-\lambda}\right)^{\frac{2+M-N}{2}} \left(\frac{\hat{r}}{2R_1}\right)^N F_I \tag{26}$$

Consequently, by (20)–(22) and (26),

$$\Sigma_{ik} = -\frac{3DZ_0}{S_1^2}\int_{S_1} \mathrm{d}S_1 \{F_I \lambda n_i n_k\} \times \left[1 + \frac{C}{2Z_0R_1}\int_{2R_1}^{2R_1/\lambda} \mathrm{d}\hat{r}\left\{\left(\frac{1-\lambda\hat{r}/2R_1}{1-\lambda}\right)^{\frac{2+M-N}{2}}\left(\frac{\hat{r}}{2R_1}\right)^{N+1}\right\}\right] \tag{27}$$

The integral with respect to $\hat{r}$ is difficult to evaluate analytically in general. However, the integral may be represented accurately by its asymptotic expansion for $1-\lambda \ll 1$, giving

$$\Sigma_{ik} = -\frac{3DZ_0}{S_1^2}\int_{S_1} \mathrm{d}S_1 \left\{1 + \frac{2C(1-\lambda)}{Z_0\lambda^{N+2}}\left[\frac{1}{4+M-N} - \frac{(N+1)(1-\lambda)}{6+M-N}\right]\right\} F_I \lambda n_i n_k \tag{28}$$

with F_I computed from eqn (23). This integration is exact when $N = 0$ (i.e. the rate independent limit).

In addition to calculation of macroscopic stress, the number of contacts Z and the total area of contact A_t for a representative particle follow directly from the assump-

tions of affine deformation, eqns (1)–(4) and indentation theory, eqn (14). Recall that $\mathrm{d}G/S_1$ particles per unit area of reference sphere initially have their centres between $\hat{r}$ and $(\hat{r}+\mathrm{d}\hat{r})$ from the reference particle. The indentation overlap h for these neighbouring particles is given by eqn (4) and the associated radius of contact a is specified by eqn (14), with $R_0 = R_1/2$. The total area of contact A_t for a representative particle follows as

$$A_t = \frac{1}{S_1}\int_{S_1} \mathrm{d}S_1 \int_{2R_1}^{2R_1/\lambda} \mathrm{d}\hat{r}\frac{\mathrm{d}G}{\mathrm{d}\hat{r}}\pi a^2 \tag{29}$$

Upon substituting for G from eqn (21), and performing the integration in eqn (29) with respect to $\hat{r}$, we find that A_t is given by

$$A_t = \frac{c^2}{4}\int_{S_1} \mathrm{d}S_1 \left\{2Z_0(1-\lambda)+C\left(\lambda+\frac{1}{\lambda}-2\right)\right\} \tag{30}$$

The number of contacts per particle Z follows directly as

$$Z = \frac{1}{S_1}\int_{S_1} \mathrm{d}S_1 \int_{2R_1}^{2R_1/\lambda} \mathrm{d}\hat{r}\frac{\mathrm{d}G}{\mathrm{d}\hat{r}} = Z_0 + \frac{C}{S_1}\int_{S_1} \mathrm{d}S_1 \left(\frac{1}{\lambda}-1\right) \tag{31}$$

by eqn (21).

In the limiting case of infinitesimal straining, the stretch ratio λ simplifies to $\lambda \approx 1+E_{ij}n_in_j$, where $\mathbf{E}$ is the macroscopic infinitesimal strain tensor. This limit is valid for small amounts of consolidation and is likely to be broadly applicable since the relative density of interest will generally range from $D = D_0 = 0.64$ to $D = 0.80$, say. At about 80% relative density, the three-dimensional, network of porosity begins to close off into isolated voids and there is a transition to Stage II in which the closure of cavities rather than the flattening of isolated junctions controls the deformation (Helle et al., 1985). For the case of infinitesimal straining, h_I and $\dot{h}_I$ are evaluated from linear strain kinematics, and follow from eqns (24) and (25) as

$$h_I = -2R_1 n_i E_{ij} n_j \tag{32}$$

and

$$\dot{h}_I = -2R_1 n_i \dot{E}_{ij} n_j \tag{33}$$

respectively. Additionally, if the number of contacts is kept constant then the term in curly brackets in eqn (28) reduces to unity, and eqn (28) simplifies to

$$\Sigma_{ik} = -\frac{3\eta D_0 Z_0}{S_1^2}(2R_1)^{\frac{2+M+N}{2}}\int_{S_1} \mathrm{d}S_1[(-n_jE_{jl}n_l)^{\frac{2+M-N}{2}}(-n_p\dot{E}_{pq}n_q)^N n_in_k] \tag{34}$$

Of particular interest is the result for $N = M = 0$, which is the rate independent non-hardening result. This gives

$$\Sigma_{ij} = \left(\frac{6\eta D_0 Z_0 R_1}{S_1^2}\right) \int_{S_1} \mathrm{d}S_1 [n_i n_j n_k n_l E_{kl}] \tag{35}$$

which simplifies to

$$\Sigma_{ij} = \left(\frac{\eta D_0 Z_0}{5\pi R_1}\right) \left[E_{ij} + \frac{1}{2}\delta_{ij} E_{kk} \right] \tag{36}$$

upon use of the identity (see for example, Ogden, 1984),

$$\int_{S_1} \frac{\mathrm{d}S_1}{S_1} [n_i n_j n_k n_l] = \frac{1}{15}(\delta_{ij}\delta_{kl} + \delta_{ik}\delta_{jl} + \delta_{il}\delta_{jk}) \tag{37}$$

The suggested values for the parameters in eqn (36) (i.e. $\eta = 3\pi c^2 \sigma_1 R_1$, $c^2 = 1.43$, $Z_0 = 7.3$) lead to

$$\Sigma_{ij} = 6.3\sigma_1 D_0 [E_{ij} + \tfrac{1}{2} E_{kk}\delta_{ij}] \tag{38}$$

The form of eqn (38) is equivalent to that of an isotropic linear elastic law with a Young's modulus equal to $7.8\sigma_1 \mathrm{D}_0$ and a Poisson ratio of 0.25. The use of a fixed value of D_0 is consistent with asymptotic expansions which lead to the linearised form of eqn (38). The conclusion, therefore, is that rigid, ideally plastic powders experiencing consolidations which generate monotonic compressive loads on all junctions respond macroscopically as if they are linear elastic and isotropic. A predicted value for the Poisson's ratio of 0.25 is a direct consequence of the assumption of frictionless contact : only central forces act between particles, and shear and bending loads are neglected. This is reminiscent of the rari-constant theory of elasticity, as summarised by Love (1927). We further note in passing that Shima and Oyane (1976) measured a 'plastic Poisson ratio' of 0.25–0.3 in the uniaxial compression of copper powder.

For infinitesimal straining but arbitrary N and M, expressions for the total area of contact A_t and number of contacts per particle Z simplify from eqns (30) and (31) to

$$A_\mathrm{t} = -\frac{c^2}{6} Z_0 E_{kk} S_1 \tag{39}$$

and

$$Z = Z_0 \tag{40}$$

3.1. *Isostatic compaction*

In isostatic compaction of homogeneous spherical powder, both F_I and λ are independent of **n**. The stretch ratio is given by

$$\lambda = (D_0/D)^{1/3} \tag{41}$$

where it is assumed that pressure-driven compaction commences at random dense packing. Similarly, the rate of change of λ is

$$\dot{\lambda} = -\frac{1}{3}\left(\frac{D_0}{D}\right)^{1/3}\frac{\dot{D}}{D} \tag{42}$$

Consequently, the indentation h_I for junctions initially in contact is

$$h_I = 2R_1[1-(D_0/D)^{1/3}] \tag{43}$$

by eqns (24) and (41), and likewise

$$\dot{h}_I = \frac{2R_1}{3}\left(\frac{D_0}{D}\right)^{1/3}\frac{\dot{D}}{D} \tag{44}$$

by (25) and (42). It follows from eqn (23) that

$$F_I = \eta(2R_1)^{\frac{2+M+N}{2}}[1-(D_0/D)^{1/3}]^{\frac{2+M-N}{2}}\left[\left(\frac{D_0}{D}\right)^{1/3}\frac{\dot{D}}{3D}\right]^N \tag{45}$$

On noting the identity

$$\int_{S_1} n_i n_k \,\mathrm{d}S_1 = \frac{1}{3}S_1\delta_{ik} \tag{46}$$

the macroscopic stress can be written in the form

$$\Sigma_{ik} = -P\delta_{ik} \tag{47}$$

where, from eqns (28) and (45), the pressure P required to compress the aggregate is

$$P = \frac{\kappa\eta D Z_0}{S_1}(2R_1)^{\frac{2+M+N}{2}}\left[1-\left(\frac{D_0}{D}\right)^{1/3}\right]^{\frac{2+M-N}{2}}\left(\frac{D_0}{D}\right)^{\frac{N+1}{3}}\left(\frac{\dot{D}}{3D}\right)^N \tag{48}$$

and

$$\kappa \equiv 1+\frac{2C}{Z_0}\left(\frac{D}{D_0}\right)^{\frac{N+2}{3}}\left[1-\left(\frac{D_0}{D}\right)^{1/3}\right]\left\{\frac{1}{4+M-N}-\frac{(N+1)[1-(D_0/D)^{1/3}]}{6+M-N}\right\} \tag{49}$$

The densification rate $\dot{D}$ can be obtained from eqn (48) by rearrangement, which shows that for any pressure P, $\dot{D}$ is infinite at random dense packing ($D = D_0$). For the rate independent case, $N = 0$, graphs of the pressure P vs the density D for selected values of M are shown in Fig. 4. The plots are terminated at the transition to Stage II at $D = 0.80$. It should be noted that the results in Fig. 4 are relatively sensitive to the strain hardening exponent M. This sensitivity of macroscopic pressure to M is associated with the strong dependence of η on M, and can be explained as follows. Since the level of effective strain in the vicinity of each contact is much less than unity, the flow stress distribution is much less than σ_0 and increases steeply with depth of indentation.

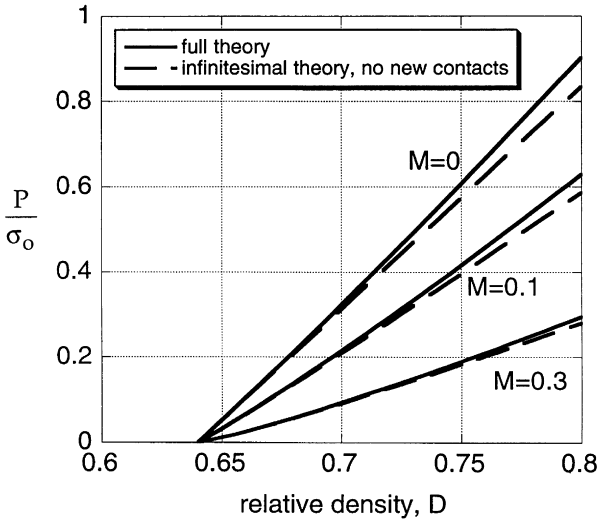

Fig. 4. Macroscopic pressure vs density for rate independent plasticity during isostatic compaction. $N = 0$.

For the rate dependent but non-hardening case ($M = 0$) the pressure P, normalised by $(\dot{D}/D)^N$, is plotted against relative density in Fig. 5. The plots are extended up to $D = 0.80$ as before. The rigid, ideally plastic limit $N = 0$ is included in the figure.

The parameter κ in eqn (49) equals unity when the effects of new contacts during

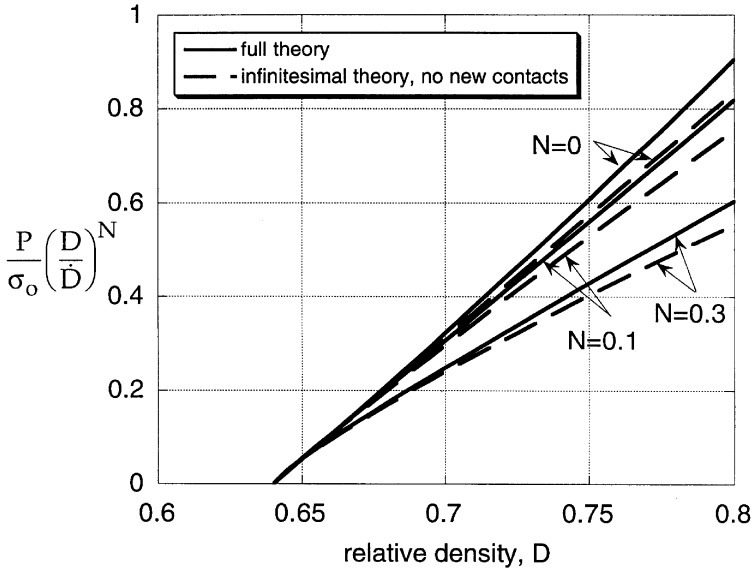

Fig. 5. Macroscopic pressure at a given densification rate vs relative density for a power law creeping material during isostatic pressing. $M = 0$.

compaction are neglected. Inspection of eqn (49) shows that up to $D = 0.80$, κ differs little from unity and the effects of new contacts can be neglected. For example, in the rigid, perfectly plastic limit $N = M = 0$, with $D_0 = 0.64$, $D = 0.80$, $C = 15.5$ and $Z_0 = 7.3$, the parameter $\kappa = 1.08$, and the error in P by neglecting new contacts is only 8%.

It is instructive to compare the predictions of the kinematically non-linear theory presented above with the version neglecting new contacts and assuming infinitesimal strain. Upon specialising eqn (34) to the isostatic limit, the pressure P is given by

$$P = \frac{\eta D_0 Z_0}{\pi}(2R_1)^{\frac{M+N-2}{2}}\left[\left(\frac{D-D_0}{3D_0}\right)^{\frac{2+M-N}{2}}\left(\frac{\dot{D}}{3D_0}\right)^{N}\right] \tag{50}$$

Note that the effect of new contacts is not present in the infinitesimal strain version, but this leads to negligible error as discussed above. The predictions of the infinitesimal strain (50) are in good agreement with those of the full theory, as seen by the direct comparisons shown in Figs 4 and 5. A detailed inspection of relations (48) and (50) reveals that the small difference between the two predictions arises mainly from the strengthening contribution of new contacts and not from the effect of non-linear kinematics vs linear kinematics.

For completeness, the total area of contact A_t and number of contacts Z for a representative particle in the isostatic case are obtained from eqns (30) and (31) for the full non-linear theory, giving

$$A_t = \frac{c^2}{4}\left\{2Z_0\left[1-\left(\frac{D_0}{D}\right)^{1/3}\right]+C\left[\left(\frac{D_0}{D}\right)^{1/3}+\left(\frac{D}{D_0}\right)^{1/3}-2\right]\right\}S_1 \tag{51}$$

and

$$Z = Z_0 + C\left[\left(\frac{D}{D_0}\right)^{1/3}-1\right] \tag{52}$$

In the limit of infinitesimal straining these expressions simplify to the previous results eqns (39) and (40), respectively.

3.2. *Closed die compaction*

In addition to isostatic compaction, closed die compaction is of major industrial relevance, particularly in the powder metallurgy industry. A typical processing route is to cold-compact metallic powder along the major axis of a cylindrical closed die, later followed by sintering at elevated temperature and at atmospheric pressure. Alternatively, the compaction and sintering processes are combined in a single hot compaction operation. The case of closed die compaction has been studied previously by Fleck et al. (1997), and only the main results are summarised below.

In closed die compaction, with the compression direction parallel to the x_3-axis, the components of the deformation gradient are given by

$$F_{ij} = \delta_{ij} \tag{53}$$

except that

$$F_{33} = \Lambda \tag{54}$$

where Λ is the compaction ratio. With ϕ being the angle between a given orientation and the x_3-axis as shown in Fig. 1, eqn (3) provides

$$\lambda^{-2} = 1 + (\Lambda^{-2} - 1)\cos^2\phi \tag{55}$$

This result can be used in eqns (24) and (25) to give $h_I(\phi)$, and $\dot{h}_I(\phi)$. $F_I(\phi)$ then follows from eqn (23). In addition,

$$D/D_0 = 1/\Lambda \tag{56}$$

where, as before, it is assumed that compaction commences at random dense packing.

The results above, along with eqn (28), have been used to compute $S = \Sigma_{33}$ and $T = \Sigma_{11} = \Sigma_{22}$ for closed die compaction, for two values of the strain hardening exponent M in the rate independent limit ($N = 0$). The results are shown in Fig. 6 plotted against the relative density. As for the case of isostatic compaction, the results are sensitive to the strain hardening exponent M, but examination of eqn (28) reveals that most of the sensitivity is accounted for by η. The level of macroscopic stress at each density depends on the area of junctions produced by the deformation and on the average indentation pressure at each contact. As the contact area between particles is non-uniform with respect to relative orientation of particles, the axial stress S differs significantly from the transverse stress T. The larger indentations and junctions near

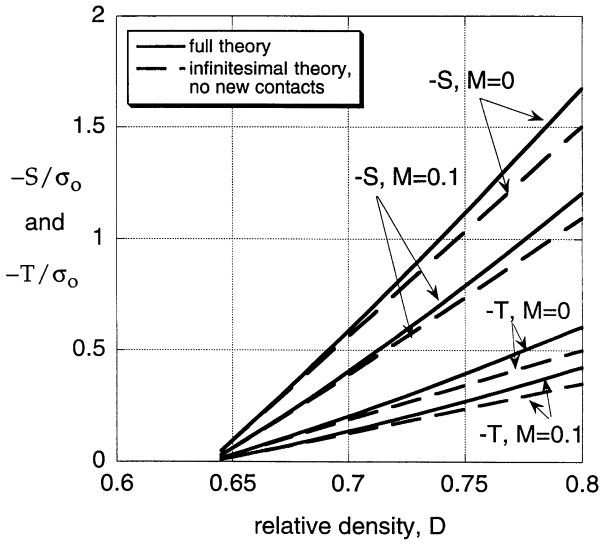

Fig. 6. Macroscopic stress vs relative density for rate independent plasticity during closed die compaction. $N = 0$.

the poles of the reference sphere compared to near the equator lead to an axial stress that is larger than the transverse stress. For example, in the initial stages of compaction of a rigid, perfectly plastic solid the magnitude of the axial stress is three times that of the transverse stress, as follows from eqn (36) and as discussed earlier by Fleck et al. (1997).

The results for S and T from infinitesimal strain theory, eqn (34), have been plotted in Fig. 6 for comparison. In this case

$$n_i E_{ij} n_j = (\Lambda - 1)\cos^2\phi \tag{57a}$$

and

$$n_i \dot{E}_{ij} n_j = \dot{\Lambda}\cos^2\phi \tag{57b}$$

The axial stress Σ_{33} can be obtained in closed form by integration of eqn (34) over S_1, giving

$$S \equiv \Sigma_{33} = \frac{-1}{5+M+N}\frac{3\eta D_0 Z_0}{\pi}(2R_1)^{\frac{M+N-2}{2}}\left(\frac{D-D_0}{D_0}\right)^{\frac{2+M-N}{2}}\left(\frac{\dot{D}}{D_0}\right)^N \tag{58}$$

The transverse stress T is obtained by numerical integration of eqn (34). It can be seen from Fig. 6 that these results for infinitesimal straining approximate the finite deformation results fairly well. Further details on the comparison between the finite strain and infinitesimal strain results are given by Fleck et al. (1997) in the limiting case $M = N = 0$, for both closed die compaction and isostatic compaction.

The axial stress S, normalised by $(\dot{D}/D)^N$, is plotted in Fig. 7 against relative density for closed die compaction, upon taking $M = 0$. The response is displayed for selected

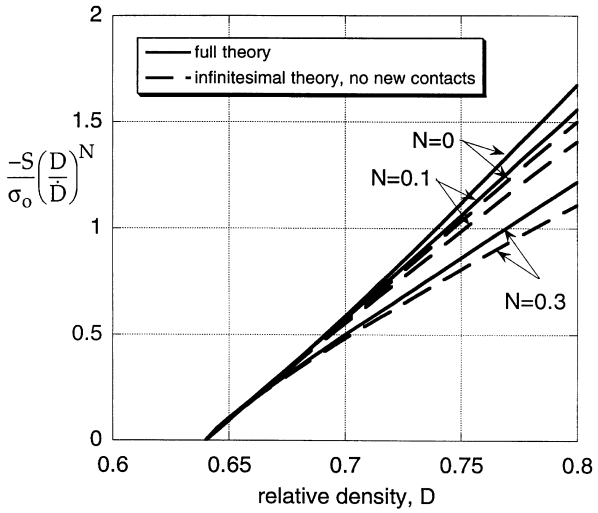

Fig. 7. Macroscopic axial stress at a given densification rate vs relative density for a power law creeping material during closed die compaction. $M = 0$.

values of the creep exponent N, including the rigid, ideally plastic limit, $N = 0$. Plots are given both for the finite strain result eqn (28) and for the infinitesimal strain case, eqn (34). Again, it can be seen that the simpler infinitesimal theory approximation of eqn (34) predicts the more exact results from eqn (28) quite well.

3.3. *Yield surfaces*

For the rate independent case, $N = 0$, all combinations of macroscopic stress which cause further deformation for a given state of the powder aggregate can be computed from eqn (28) to predict a yield surface. Plastic flow is normal to the yield surface, as discussed by Fleck et al. (1992), following the general proof outlined by Gurson (1977).

The current state of the powder is characterised by $h_I(\mathbf{n})$ as given by eqn (24), with $\lambda(\mathbf{n})$ determined by the prior deformation $\mathbf{F}$ via eqn (3). At further yield, the junction load F_I in eqn (28) is computed for any instantaneous macroscopic strain rate applied to the aggregate. The junction load F_I for use in the yield stress calculation is given by eqn (23) (with $N = 0$) if the junction continues to experience compression; i.e. $\dot{h}_I > 0$ from eqn (25). For a given orientation, if $\dot{h}_I \leqslant 0$ due to the imposed deformation rate, so that a junction separates or there is no relative motion across it, a different choice is made for F_I. If $\dot{h}_I = 0$, we enforce $F_I = 0$ since no deformation rate is imposed at the contact of interest. If the powder is cohesionless, F_I vanishes when $\dot{h}_I < 0$ because separation of the powder particles is not resisted. If there is full cohesion between the particles and $\dot{h}_I < 0$, F_I is given by the negative of eqn (23) (with $N = 0$), since the junction sustains a tensile load.

In summary, the procedure to compute a yield surface is first to generate a current state by a monotonic deformation and then to impose a full range of direction of subsequent deformation rates on that current state. The stresses for each direction of deformation rate are computed from eqn (28) using the procedure outlined above for evaluating F_I at each orientation. The resulting locus of stresses from eqn (28) defines the current yield surface in macroscopic stress space $\mathbf{\Sigma}$. A similar procedure can be used with eqn (34) to determine the yield surface based on infinitesimal strain theory.

We shall restrict our presentation of results to the axisymmetric case. Yield surfaces after prior isostatic consolidation from $D_0 = 0.64$ to $D = 0.70$ are shown in Fig. 8, and after prior closed die compaction in Fig. 9. Results with and without cohesion are depicted for various hardening exponents M and are computed from eqn (28). The yield surfaces are plotted as contours of effective stress $\Sigma = S - T$ vs mean stress $\Sigma_m = \frac{1}{3}S + \frac{2}{3}T$ for axisymmetric states of stress. Associated flow prevails for the macroscopic aggregate, so that the macroscopic deformation rate $\mathbf{D}$ is normal to the yield surface. In Fig. 8 and in subsequent figures, the components of the deformation rate are the dilatancy $\dot{H} \equiv 2\dot{E}_{11} + \dot{E}_{33}$ (parallel to the abscissa) and the deviatoric strain rate $\dot{E} \equiv 2(\dot{E}_{33} - \dot{E}_{11})/3$ (parallel to the ordinate). The yield surfaces for the perfectly plastic case $M = 0$ are the same shape as predicted in our previous work on isostatic compaction (Fleck et al., 1992a; Fleck, 1995). The vertices at the loading point on the yield surfaces on the hydrostatic stress axis have been discussed already in these papers.

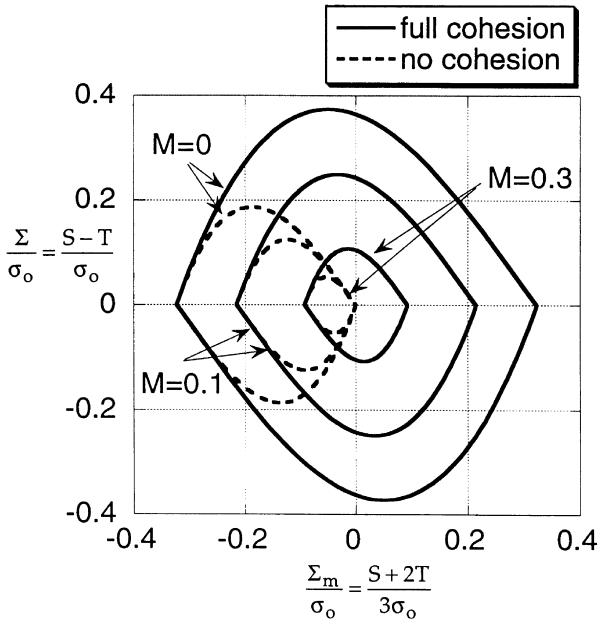

Fig. 8. Yield surfaces after isostatic compaction to a relative density of 70% for rate independent plasticity of a cohesive and a cohesionless aggregate. $N = 0$.

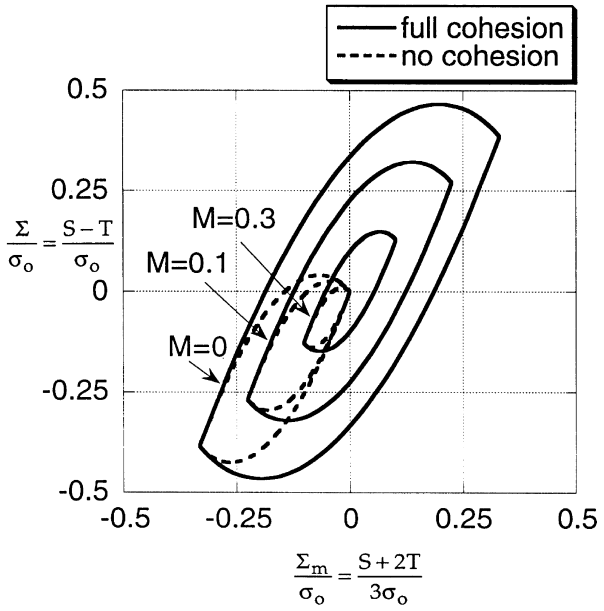

Fig. 9. Yield surfaces after closed die compaction to a relative density of 70% for rate independent plasticity of a cohesive and a cohesionless aggregate. $N = 0$.

Yield surfaces after prior closed die compaction from $D_0 = 0.64$ (i.e. $\Lambda = 1$) to $D = 0.70$ (i.e. $\Lambda = 0.914$) are shown in Fig. 9. They are computed from eqn (28) and results with and without cohesion are given for various strain hardening exponents. The yield surface for the perfectly plastic case, $M = 0$, is essentially the same as that given previously for prior closed die compaction by Fleck (1995) and represents the shape of all the yield surfaces quite well. Fleck (1995) compared his predictions with experimental data on closed die compaction reported elsewhere in the literature and found good agreement. More recently, Akisanya et al. (1997) have performed triaxial tests on copper powders and find that closed die compaction gives strong anisotropy in comparison with isotropic compaction, with the formation of a corner at the loading point. The model of Fleck (1995) gives similar predictions to those reported here, and was found to be in excellent agreement with the measurements of Akisanya et al. (1997).

The vertices on the yield surfaces in Fig. 9 lie at the loading point associated with closed die compaction and at its image at the opposite end of the yield surface. The elongation of the yield surface in Fig. 9 compared to those in Fig. 8 is caused by the larger indentations and larger junction areas near the poles of the reference particle which make the aggregate strong in response to deformation rates close to uniaxial strain. On the other hand, deformation rates orthogonal to the uniaxial strain direction are resisted mainly by junctions which are mildly indented and therefore have relatively small areas. As a result, the yield surface is relatively narrow in the second and fourth quadrants giving rise to a weak response to deformation rates close to axisymmetric plane strain. It may be further concluded from Figs 8 and 9 that the shapes of the respective yield surfaces do not vary much with the hardening exponent; the major factor dictating yield surface shape is the geometry of local contacts.

Yield surfaces at $D = 0.70$ for the perfectly plastic case for both prior isostatic consolidation and for prior closed die compaction are shown in Fig. 10 for a powder with full cohesion. Results are given for the complete model computed from eqn (28), for the model when new contacts are ignored [i.e. eqn (28) with $C = 0$] and for infinitesimal strain theory with no new contacts, eqn (34). It can be seen that at $D = 0.70$ there is little difference among these predictions. This suggests that the infinitesimal strain theory, which also neglects the formation of new contacts, is adequate at this relative density. The discrepancies among the models increases with relative density, but even at $D = 0.80$ the differences are modest, as was already noted in the remarks associated with Fig. 4.

3.4. *Creep dissipation surfaces*

For the case of a viscoplastic aggregate (any M and $N \neq 0$), eqn (28) is used to calculate the locus of values of macroscopic stress which give rise to the same dissipation rate for a given state of the powder aggregate. This locus forms a surface of constant dissipation. The procedure is similar to that used for computing the yield surface: first, a current state is generated by contact growth under fixed macroscopic stress to a desired level of relative density D and second, a range of subsequent virtual deformation rates is imposed on the powder and the associated macroscopic stress

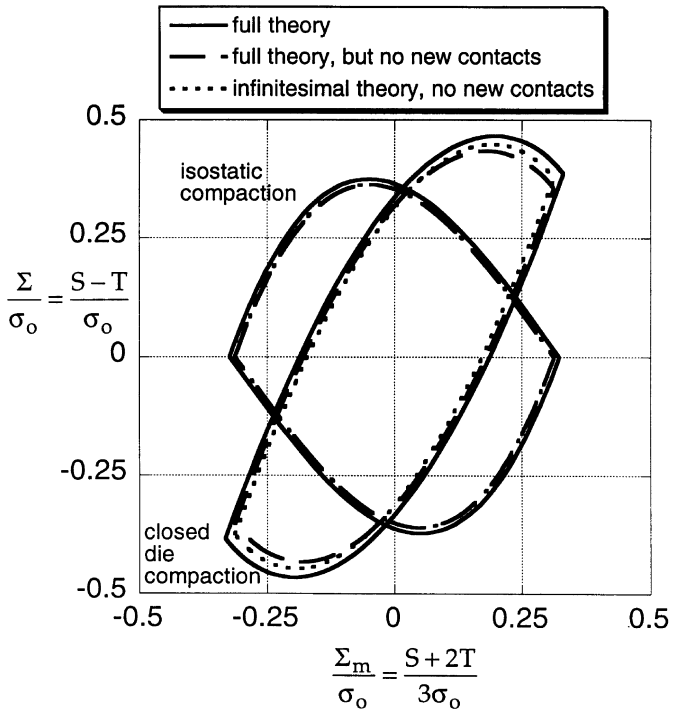

Fig. 10. Yield surfaces after compaction to a relative density of 70% for the rigid, ideally plastic limit of a cohesive aggregate showing results for various versions of the model. $M = N = 0$.

states are computed from eqn (28). The load F_I on a junction is computed according to eqn (23). For the case of full cohesion between particles, F_I is compressive, tensile or vanishes according to whether a junction experiences continued indentation, separation or is not deforming under the imposed virtual deformation rate **D**. The absolute value of $\dot{h}_I$ is used in eqn (23) and the sign of F_I is made to agree with the sign of $\dot{h}_I$. Tensile loads are excluded for cohesionless powder as before.

For each macroscopic virtual deformation rate **D** about the current state, the creep dissipation per unit volume of aggregate $\dot{W}^c$ is computed as

$$\dot{W}^c = \Sigma_{ij} D_{ij} \tag{59}$$

The magnitude of the virtual deformation rate is then scaled until $\dot{W}^c$ equals the same prescribed value for all directions of virtual deformation rate imposed on the current powder aggregate. The macroscopic stress corresponding to each direction of virtual deformation rate is calculated and plotted as a surface of constant dissipation in stress space. A similar procedure can be used with eqn (34) to determine the dissipation surfaces based on infinitesimal strain theory.

It is convenient to introduce a stress potential $\Psi(\boldsymbol{\Sigma})$ which is the dual of the creep potential $\Phi(\dot{\mathbf{D}})$, defined by

$$\Psi(\boldsymbol{\Sigma}) = \sup_{D_{ij}} [\Sigma_{ij} D_{ij} - \Phi(\mathbf{D})] \tag{60}$$

The stress potential $\Psi(\boldsymbol{\Sigma})$ can be stated directly as

$$\Psi(\boldsymbol{\Sigma}) = \int_{\Sigma^*_{ij}=0}^{\Sigma^*_{ij}=\Sigma_{ij}} D_{ij}(\boldsymbol{\Sigma}^*)\, \mathrm{d}\Sigma^*_{ij} \;\Leftrightarrow\; D_{ij} = \frac{\partial \Psi(\mathbf{F}, \boldsymbol{\Sigma})}{\partial \Sigma_{ij}} \tag{61}$$

It is evident that the deformation rate $\mathbf{D}$ is normal to the potential surface $\Psi(\boldsymbol{\Sigma})$ in stress space, and that Ψ is homogeneous and of degree $(N+1)/N$ in $\boldsymbol{\Sigma}$. Following the argument of Rice (1970) it is straightforward to show that $\Psi(\boldsymbol{\Sigma})$ is convex provided the indentation rate at each contact between particles increases with increasing contact load. Furthermore, in the rate independent limit ($N \to 0$), the macroscopic yield surface displays both convexity and normality.

The stress potential $\Psi(\boldsymbol{\Sigma})$ is related directly to the dissipation $\dot{W}^{\mathrm{c}}$ by

$$\Psi = \frac{N}{N+1} \dot{W}^{\mathrm{c}} \tag{62}$$

Thus, $\dot{W}^{\mathrm{c}}$ is homogeneous and of degree $(N+1)$ in $\boldsymbol{\Sigma}$. In the spirit of Calladine and Drucker (1962) it is convenient to introduce a macroscopic effective stress $\bar{\Sigma}$ which is homogeneous and of degree one in $\boldsymbol{\Sigma}$ such that $\dot{W}^{\mathrm{c}}$ depends only upon the scalar $\bar{\Sigma}$, viz

$$\dot{W}^{\mathrm{c}}(\Sigma_{ij}) \equiv \sigma_0 \left(\frac{\bar{\Sigma}(\Sigma_{ij})}{\sigma_0} \right)^{\frac{N+1}{N}}. \tag{63}$$

Creep dissipation surfaces in stress space are presented below in the form of contours of $\bar{\Sigma}/\sigma_0 = 1$. In the limit of $N \to 0$, the macroscopic yield surface for the rigid, perfectly plastic solid is recovered, as discussed by Cocks (1994).

Representative results are now given for the case of prior isostatic consolidation from $D_0 = 0.64$ to $D = 0.70$; the resulting creep dissipation potential surfaces are shown in Fig. 11. Results with and without cohesion are depicted for the non-hardening case $M = 0$ for various creep exponents N and are computed from eqn (28). The shape of the creep dissipation surfaces for values of N close to zero are in close agreement with those given by Kuhn and McMeeking (1992) for isostatic compaction with full cohesion.

Creep dissipation surfaces after prior closed die compaction from $D_0 = 0.64$ to $D = 0.70$ are computed from eqn (28) and are plotted in Fig. 12. The surfaces are displayed for both cohesion and no cohesion, with $M = 0$ and with various creep exponents N. The elongated shape arises from the anisotropy of indentations and junction areas around particles caused by the prior uniaxial strain. There is a strong resemblance with the corresponding yield contours in Fig. 9, and the shapes of the dissipation surfaces do not vary much with the creep exponent N. In the limit $N = 0$, the dissipation surface reduces to the yield surface for perfect plasticity with vertices, as noted above.

Creep dissipation surfaces are compared for prior isostatic consolidation and for

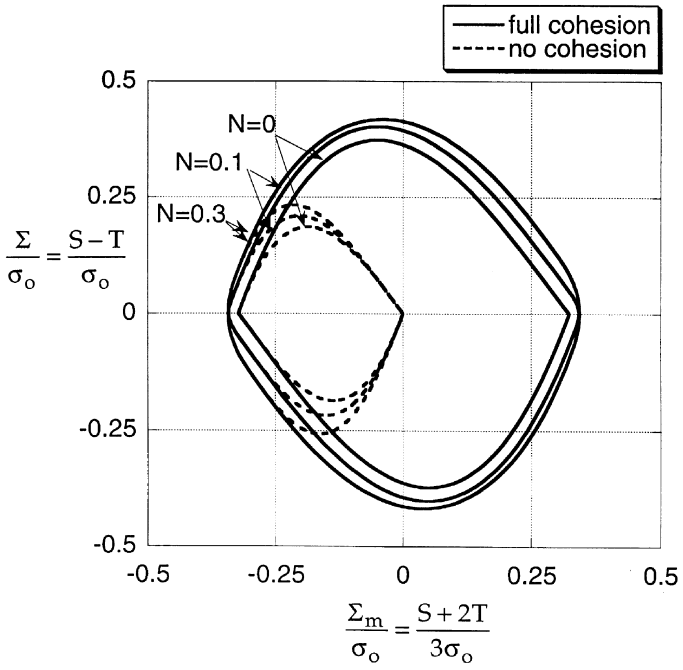

Fig. 11. Contours of creep dissipation after isostatic compaction to a relative density of 70% for the power law creep of a cohesive and a cohesionless aggregate. $M = 0$.

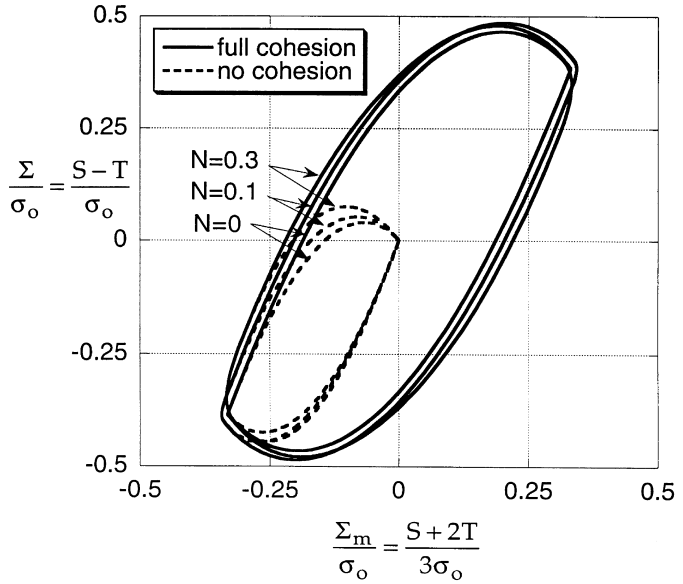

Fig. 12. Contours of creep dissipation after closed die compaction to a relative density of 70% for the power law creep of a cohesive and a cohesionless aggregate. $M = 0$.

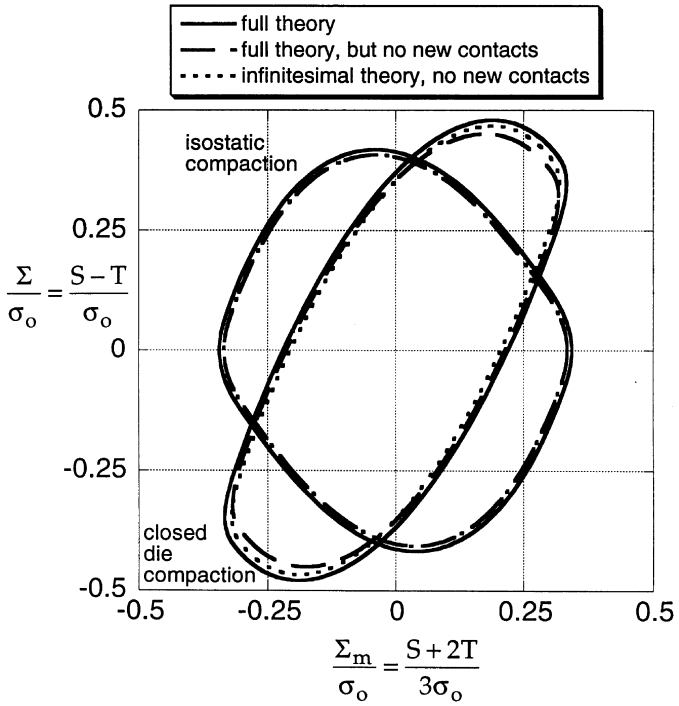

Fig. 13. Contours of creep dissipation after compaction to a relative density of 70% for the power law creep of a cohesive aggregate showing results for various versions of the model. $M = 0$, $N = 0.3$.

prior closed die compaction in Fig. 13 for a powder with full cohesion; we take $D_0 = 0.64$, $D = 0.70$, $M = 0$ and $N = 0.3$. Dissipation surfaces are given for the complete model from eqn (28), for the model when new contacts are ignored [i.e. eqn (28) with $C = 0$] and for infinitesimal strain theory, eqn (34). Again, there is little difference between the predictions of the full theory and the infinitesimal version. This suggests that the infinitesimal strain theory, which also neglects the formation of new contacts, is adequate for a small amount of compaction. The discrepancies among the models increase with relative density, but even at $D = 0.80$, the differences can be neglected for practical purposes, as was noted in the remarks associated with Figs 4 and 5.

4. Composite powders

So far we have derived constitutive relations for a monolithic powder. Now consider a mixture of n spheres comprising two populations of particles: type 1 having strength σ_1 and radius R_1, and type 2 having strength σ_2 and radius R_2. We seek the macroscopic compaction response of the aggregate under multi-axial loading.

The strength ratio k is defined by

$$k = \sigma_2/\sigma_1 \tag{64}$$

and the size ratio by

$$\rho = R_2/R_1 \tag{65}$$

Let f_1 be the number fraction of type 1 particles and f_2 that of type 2 so that

$$f_1 + f_2 = 1 \tag{66}$$

The indentations for each junction are controlled by the local contact force and the hardnesses and sizes of the particles. We need to distinguish between the interpenetration h at the various types of contact: we express the overlap between two neighbouring type 1 particles by h_{11}, the overlap between two neighbouring type 2 particles by h_{22}, and the overlap between a type 1 particle and a type 2 particle by h_{12} or, equivalently, by h_{21}. We shall denote the various types of overlap using notation $h_{\alpha\beta}$, with the Greek subscripts α and β ranging from 1–2. Here, a repeated Greek suffix does not imply summation. In similar fashion, the contact force is labelled $F_{\alpha\beta}$, and the centre–centre spacing of two contacting particles is designated by

$$R_{\alpha\beta} \equiv R_\alpha + R_\beta \tag{67}$$

We shall calculate the compaction response for the mixture of particles. In view of the prior discussion, we assume infinitesimal strain kinematics so that $\lambda \approx 1$ and we neglect the formation of new contacts. The macroscopic stress for a two phase composite follows from eqn (19) as

$$\Sigma_{ij} = -\frac{1}{V}\sum_J \{F_{\alpha\beta} R_{\alpha\beta} n_i n_j\}_J \tag{68}$$

where the summation is taken over all contacts J, in a composite of volume V.

It remains to determine the contact force distribution $F_{\alpha\beta}(\mathbf{n})$. In general, more or less sophisticated trial functions can be used, but here a straightforward Reuss approach is adopted such that all junctions transmit the same force at all particulate contacts in a given direction $\mathbf{n}$. A prototype model of this kind for isostatic compaction of a powder composite was used by Bouvard (1993) for equally sized populations of creeping and rigid particles. Accordingly, for identical contact forces $F_{12}(\mathbf{n}) = F_{22}(\mathbf{n}) = F_{11}(\mathbf{n})$.

Upon introducing contact co-ordination numbers, Z_{11} is, on average, the number of contacts each type 1 particle makes with other type 1 particles, Z_{12} is the average number each type 1 particle makes with type 2 particles, and so on. Note that $f_1 Z_{12} = f_2 Z_{21}$, and the average co-ordination number of all particles Z_C is given by

$$Z_C = f_1(Z_{11} + Z_{12}) + f_2(Z_{21} + Z_{22}). \tag{69}$$

The subscript C here and elsewhere refers to the composite. Thus, (68) can be expressed explicitly as

$$\Sigma_{ij} = -\frac{2}{Z_C V}\sum_J \{n_i n_j [f_1 Z_{11} R_1 F_{11} + f_1 Z_{12}(R_1 + R_2) F_{12} + f_2 Z_{22} R_2 F_{22}]\}_J \tag{70}$$

for a statistically homogeneous, uncorrelated and isotropic mixture. Turner and Ashby (1995a, b) provide the following estimates:

$$Z_{11} = \frac{f_1}{(f_1+f_2\rho)^2} Z_C$$

$$Z_{12} = \frac{f_2\rho}{(f_1+f_2\rho)^2} Z_C$$

$$Z_{21} = \frac{f_1\rho}{(f_1+f_2\rho)^2} Z_C$$

$$Z_{22} = \frac{f_2\rho^2}{(f_1+f_2\rho)^2} Z_C \tag{71}$$

in terms of the average co-ordination number Z_C over all particles. Further, Turner and Ashby (1995) suggest that Z_C satisfies the empirical law

$$Z_C = 12D_C \tag{72}$$

where D_C is the initial relative density of the aggregate. Upon using the estimates (70) and (71), the macroscopic stress in (70) reduces to

$$\Sigma_{ij} = -\frac{2R_1}{V}\frac{(f_1+f_2\rho^2)}{(f_1+f_2\rho)}\sum_J \{n_i n_j F_{11}\}_J \tag{73}$$

For future use, this relation is re-written in the alternative form,

$$\Sigma_{ij} = -\frac{3D_C Z_C}{4\pi R_1^2}\frac{(f_1+f_2\rho^2)}{(f_1+f_2\rho)(f_1+f_2\rho^3)}\int_{S_1} [n_i n_j F_{11}]\frac{dS_1}{S_1} \tag{74}$$

upon (i) averaging over all orientations, (ii) noting that the volume V of the aggregate is related to the number of particles n by

$$V = \frac{4\pi R_1^3}{3}\frac{n}{D_C}(f_1+f_2\rho^3) \tag{75}$$

and upon (iii) recalling that the total number of contacts in the aggregate equals $nZ_C/2$.

The dissipation per unit volume of the composite is the sum of the dissipations at each contact,

$$\dot{W}^c = \Sigma_{ij}\dot{E}_{ij} = \frac{1}{V}\sum_J \{F_{\alpha\beta}\dot{h}_{\alpha\beta}\}_J \tag{76}$$

Once the assumption of equal local contact forces has been adopted, the indentation rates $\dot{h}_{\alpha\beta}$ may be deduced from relations (8)–(12) using the notation

$$\dot{h}_{\alpha\beta}(\mathbf{n}) \equiv \gamma_{\alpha\beta}\dot{h}_{11}(\mathbf{n}) \tag{77}$$

where the parameters $\gamma_{\alpha\beta}$ are given explicitly by

$$\gamma_{11} = 1 \tag{78a}$$

$$\gamma_{12} = \left(\frac{1+k^{-\frac{1}{M+N}}}{2}\right)^{\frac{2(M+N)}{2+M+N}} \left(\frac{1+\rho}{2\rho}\right)^{\frac{2-M-N}{2+M+N}} \tag{78b}$$

and

$$\gamma_{22} = k^{-\left(\frac{2}{2+M+N}\right)}\rho^{-\left(\frac{2-M-N}{2+M+N}\right)} \tag{78c}$$

With relation (77) in hand, the dissipation rate $\dot{W}^{c}$ can be expressed in terms of the dissipation rate between type 1 particles, by substitution of (71) and (78) into (76), and by following the same line of argument that led from (68)–(70), to obtain

$$\dot{W}^{c} = \Sigma_{ij}\dot{E}_{ij} = \frac{1}{V}\frac{(f_1^2+2f_1f_2\rho\gamma_{12}+f_2^2\rho^2\gamma_{22})}{(f_1+f_2\rho)^2}\sum_J \{F_{11}\dot{h}_{11}\}_J \tag{79}$$

To proceed, the indentation rate $\dot{h}_{11}(\mathbf{n})$ is related to the macroscopic strain rate by multiplying each side of (73) by $\dot{E}_{ij}$ and equating with the dissipation rate (79), giving

$$-\dot{E}_{ij}\frac{2R_1}{V}\frac{(f_1+f_2\rho^2)}{(f_1+f_2\rho)}\sum_J \{n_in_jF_{11}\}_J = \frac{1}{V}\frac{(f_1^2+2f_1f_2\rho\gamma_{12}+f_2^2\rho^2\gamma_{22})}{(f_1+f_2\rho)^2}\sum_J \{F_{11}\dot{h}_{11}\}_J \tag{80}$$

Since this relation holds for arbitrary F_{11}, we find

$$\dot{h}_{11} = -\frac{(f_1+f_2\rho)(f_1+f_2\rho^2)}{(f_1^2+2f_1f_2\rho\gamma_{12}+f_2^2\rho^2\gamma_{22})}2R_1(\dot{E}_{ij}n_in_j) \tag{81}$$

which integrates to give

$$h_{11} = -\frac{(f_1+f_2\rho)(f_1+f_2\rho^2)}{(f_1^2+2f_1f_2\rho\gamma_{12}+f_2^2\rho^2\gamma_{22})}2R_1(E_{ij}n_in_j) \tag{82}$$

Now F_{11} is related to h_{11} and $\dot{h}_{11}$ via $F_{11} = \eta_{11}(h_{11})^{(2+M-N)/2}(\dot{h}_{11})^N$ according to (8), and the macroscopic stress can thereby be expressed in terms of E_{ij} and $\dot{E}_{ij}$ by substitution of (81) and (82) into (74), giving

$$\Sigma_{ik} = -K\frac{3\eta_{11}D_CZ_C}{S_1^2}(2R_1)^{\frac{2+M+N}{2}}\int_{S_1} \mathrm{d}S_1[(-n_jE_{jl}n_l)^{\frac{2+M-N}{2}}(-n_p\dot{E}_{pq}n_q)^Nn_in_k] \tag{83}$$

where the constraint factor K is defined by

$$K = \frac{(f_1 + f_2\rho^2)}{(f_1 + f_2\rho^3)(f_1 + f_2\rho)} \left[\frac{(f_1 + f_2\rho)(f_1 + f_2\rho^2)}{(f_1^2 + 2f_1 f_2 \rho \gamma_{12} + f_2^2 \rho^2 \gamma_{22})} \right]^{\frac{2+M+N}{2}} \tag{84}$$

It is instructive to compare (83) with the parallel results for a monolithic power of material 1, given by (34). To avoid confusion we designate the macroscopic stress in the monolithic powder by Σ_{ij} and the macroscopic stress in the composite by Σ_{ij}^{C}. For the same value of initial relative density, and same overall co-ordination number for the composite and monolithic powder, the stress in the composite Σ_{ij}^{C} is K-times the stress Σ_{ij} in the monolithic powder.

Typically, the initial relative density for a composite D_C differs from the value D_0 for the monolithic powder, see for example Lange et al. (1991). Similarly, the average co-ordination number for the composite Z_C differs from the value Z_0 for the monolithic powder. Assume the composite and the monolithic powder are subjected to the same strain history $E_{ij}(t)$. Then, a comparison of (83) and (34) reveals that the macroscopic stress in the composite Σ_{ij}^{C} is related to the macroscopic stress Σ_{ij} in the monolithic powder by

$$\Sigma_{ij}^{C} = K_C \Sigma_{ij} \tag{85a}$$

where

$$K_C \equiv \frac{D_C Z_C}{D_0 Z_0} K \tag{85b}$$

In summary, K_C is a scalar constraint factor for the effect of the particle strength ratio σ_2/σ_1 and the size ratio R_2/R_1 upon the macroscopic strength of the composite, compared with the monolithic powder under the same strain history. In an analogous manner, if the macroscopic stress in the composite $\Sigma_{ij}^{C}(t)$ equals that for the monolithic powder $\Sigma_{ij}(t)$, then the strain history of the composite $E_{ij}^{C}(t)$ is related to that of the monolithic powder $E_{ij}(t)$ by

$$E_{ij}^{C}(t) = K_C^{-2/(2+M+N)} E_{ij}(t) \tag{86}$$

by nature of the fact that the macroscopic stress in eqn (34) is homogeneous and of degree $(2+M+N)/2$ in accumulated strain.

Clearly, the above approach gives an approximate model of the constraint. It assumes that all contacts in a given orientation carry the same indentation force irrespective of whether the contact is hard or soft. The fact that all equally oriented contacts carry the same force neglects the possibility that groups of hard particles may shield soft particles, and might induce a percolation limit. Only more thorough simulations such as by network models are likely to provide more exact constraint models. For example, from a discrete numerical model for equi-sized soft and hard spheres, Jagota and Scherer (1995) predicted percolation at a site fraction of 0.32 for the case of bonded spheres.

Of particular interest is the result for $N = M = 0$, which is the rate independent non-hardening result. The constraint factor K_C, as defined in eqns (84) and (85b), simplifies to

$$K_C = \frac{D_C Z_C}{D_0 Z_0} \frac{(f_1 + f_2\rho^2)^2}{(f_1 + f_2\rho^3)[f_1^2 + f_1 f_2(1+\rho) + f_2^2\rho/k]} \tag{87}$$

Some immediate insight into the form of K_C is achieved by specialising to the case of two populations of equi-sized spheres. Then, K_C equals K, and K_C is given by

$$K_C = \frac{1}{1 + f_2^2\left(\frac{1}{k} - 1\right)} \tag{88}$$

In the limiting case of rigid spheres of type 2, $k \to \infty$ and $K_C = (1 - f_2^2)^{-1}$. We note that the addition of a small volume fraction f_2 of rigid particle reinforcement has only a second order effect on the macroscopic stress: the constraint factor varies with f_2 according to $K_C \approx 1 + f_2^2$ for small f_2. This is consistent with the observation that the contact stiffness for a rigid particle against an ideally plastic particle is identical to that for two ideally plastic particles, as seen by direct evaluation of eqn (8).

5. Concluding discussion

The assumption of affine deformation is central to the analysis presented here, and its validity is worthy of further study. We believe that affine deformation is an adequate approximation in the Stage I regime by the following arguments. The relative density is sufficiently high for each particle to have a large number of contacting neighbours (7–10). Each particle is kinematically constrained by its neighbours so that particles are unable to roll past each other: plastic indentation and sliding occurs at contacts and the load carried by each contact is relatively uniform. In their experimental investigation, Fischmeister et al. (1978) concluded that non-radial particle motion (sliding) proceeds well into the plastic densification range of Stage I during closed die compaction. This is in sharp contrast with the behaviour of an elastic, granular material at low relative density; for such a granular solid deformation is not affine. Rather, particles tend to roll past each other and the load varies widely from contact to contact.

A separate issue is the method we have used to introduce the effect of inhomogeneity in particle size and strength. It was assumed that each junction in a given orientation carries the same load. Now, it is known that a high volume fraction of hard particles carries most of the load by percolation within a random mixture of hard and soft particles (Lange et al., 1991; Bouvard and Lange, 1991). However, when the number fraction of hard particles is modest, the approach we have used avoids the excessive weighting of the influence of the harder particles as occurs in a purely affine method. For example, if one set of particles is non-deforming, the affine method predicts that the entire powder aggregate is non-deforming for any number fraction of rigid particles. On the other hand, the prediction we have given has a finite strength except when all the particles in the aggregate are rigid.

In the analysis of composite powders a set of not more than two dissimilar spherical

particles has been studied. In reality, powder particles can be non-spherical and there is usually a wide range of sizes in a single aggregate. It remains to be seen how well our model represents non-spherical particle aggregates without sieving to limit the range of sizes. In addition, in our model, the material properties of the two families of particles can differ only in terms of the strength parameters σ_1, and σ_2, but otherwise must have the same hardening and creep exponents. As was found above, however, the shapes of the yield surfaces and creep potentials do not vary much with the material exponents. The model includes the important limiting case where one family of particles is so hard that it is essentially non-deforming. It is significant because it includes the case of ceramic inclusions placed in a metal powder to make a particulate composite.

The model developed here is strictly for the initial stages of compaction (known as Stage I) where the powder comprises identifiably separate particles, with an interpenetrating network of porosity. Consequently, the model should not be used for the later stages wherein the porosity closes off into isolated cavities. During isostatic pressing, this transition begins at about 80% relative density (Helle et al., 1985). However, before the density is reached, the deformation zones for each junction begin to influence each other and the level of constrain is affected (Akisanya et al., 1994). Therefore, it becomes necessary to modify the Stage I model which is based on non-interacting deformation zones at each junction. This is usually done by invoking an interpolation between Stages I and II (isolated porosity) models occurring over a relative density level, say 80–90% (Helle et al., 1985; Fleck et al., 1992a). However, models for Stage II, equivalent to the one presented here for Stage I, have not yet been developed.

The model we have formulated is viscoplastic and makes no allowance for elastic behaviour. It is straightforward to deduce from indentation theory that the initial Hertzian elastic contact between particles is superseded by plastic indentation when the compact has increased in density by about 1% (Larsson et al., 1996). Of a more serious nature is the effect of elasticity when the compacted aggregate is unloaded. The degree of elastic spring-back and the level of residual stress generated by unloading a non-uniformly compacted aggregate is sensitive to the details of the elastic response, and is beyond the scope of the present study.

Acknowledgement

B.S. and R.M.M. are grateful for the hospitality offered by the Cambridge Centre for Micromechanics at Cambridge University during their sabbatical leaves from the Royal Institute of Technology, Stockholm, Sweden and the University of California, Santa Barbara, U.S.A., respectively.

References

Akisanya, A.R., Cocks, A.C.F., Fleck N.A., 1994. Hydrostatic compaction of cylindrical particles. Journal of the Mechanics and Physics of Solids 42, 1067–1086.

Akisanya, A.R., Cocks, A.C.F., Fleck N A., 1997. The yield behaviour of metal powders. Int. J. Mech. Sci. 39(12), 1315–1324.

Arzt, E. (1982) The influence of an increasing particle co-ordination on the densification of spherical powders. Acta Metallurgica 30, 1883–1890.

Biwa, S., Storåkers, B., 1995. Analysis of fully plastic Brinell indentation. Journal of the Mechanics and Physics of Solids 43, 1303–1334.

Bouvard, D., 1993. On Brinell and Boussinesq indentation of creeping solids. Acta Metallurgica et Materialia 41, 1413–1420.

Bouvard, D., Lange, F.F., 1991. Relation between percolation and particle co-ordination in binary powder mixtures. Acta Metallurgica et Materialia 39, 3083–3090.

Bower, A.F., Fleck, N.A., Needleman, A., Ogbonna, N., 1993. Indentation of a power law creeping solid. Proceedings of the Royal Society of London A441, 97–124.

Calladine, C.R., Drucker, D.C., 1962. Nesting surfaces of constant rate of energy dissipation in creep. Q. Appl. Math. 20(1), 79–84.

Christoffersen, J., Mehrabadi, M.M., Nemat-Nasser, S., 1981. A micromechanical description of granular material behaviour. Journal of Applied Mechanics 48, 339–344.

Cocks, A.C.F., 1994. Overview No. 117 : The structure of constitutive laws for the sintering of fine grained materials. Acta Metallurgica et Materialia 42(7), 2191–2210.

Fischmeister, H.F., Arzt, E., 1983. Densification of powders by particle deformation. Powder Metallurgy 26, 82–88.

Fischmeister, H.F., Arzt, E., Olsson, L.R., 1978. Particle deformation and sliding during compression of spherical powders : a study by quantitative metallurgy. Powder Metallurgy 21, 179–187.

Fleck, N. A. (1995) On the cold compaction of powders. Journal of the Mechanics and Physics of Solids 43, 1409–1431.

Fleck, N.A., Kuhn, L.T., McMeeking, R.M., 1992a. Yielding of metal powder bonded by isolated contacts. Journal of the Mechanics and Physics of Solids 40, 1139–1162.

Fleck, N.A., Otoyo, H., Needleman, A., 1992b. Indentation of porous solids. International Journal of Solids and Structures 29(13), 1613–1636.

Fleck, N.A., Storåkers, B., McMeeking, R.M., 1997. The viscoplastic compaction of powders. IUTAM Symposium on Mechanics of Granular Flow and Powder Compaction, 15–17 July 1996, Cambridge, U.K., ed. N.A. Fleck, A.C.F. Cocks. Kluwer Academic Publishers, Amsterdam.

Gurson, A.L,. 1977. Continuum theory of ductile rupture by void nucleation and growth : Part I—Yield criteria and flow rules for porous ductile media. Trans. ASME J. Engng Mats and Technology 99, 2–15.

Helle, A.S., Easterling, K.E., Ashby, M.F., 1985. Hot-isostatic pressing diagrams : new developments. Acta Metallurgica 33, 2163–2174.

Hill, R., Storåkers, B., Zdunek, A.B., 1989. A theoretical study of the Brinell hardness test. Proceedings of the Royal Society of London A436, 301–330.

Jagota, A., Scherer, G.W., 1995. Viscosities and sintering rates of composite packing of spheres. Journal of the Americal Ceramics Society 78, 521–528.

Jagota, A., Dawson, P.R., Jenkins, J.T., 1988. An anisotropic continuum model for the sintering and compaction of powder packings. Mechanics of Materials 7, 255–269.

Jagota, A., Mikeska, K.R., Bordia, R.K., 1990. Isotropic constitutive model for sintering particle packings. Journal of the American Ceramics Society 73, 2266–2273.

Kuhn, H.A., Downey, C.L., 1971. Deformation characteristics and plasticity theory of sintered powder materials. International Journal of Powder Metallurgy 7(1), 15–25.

Kuhn, L.T., McMeeking, R.M., 1992. Power law creep of powder bonded by isolated contacts. International Journal of Mechanical Sciences 34, 563–573.

Lange, F.F., Atteraas, L.A., Zok, F W., 1991. Deformation consolidation of metal powder containing steel inclusions. Acta Metallurgica et Materialia 39, 209–219.

Larsson, P.-L., Biwa, S., Storåkers, B., 1996. Analysis of cold and hot isostatic compaction of spherical particles. Acta Materialia 44, 3655–3666.

Love, A.E.H., 1927. A Treatise of the Mathematical Theory of Elasticity, 4th edn. Reprinted by Dover, 1944, p. 13.

Mason, G., 1968. Radial distribution functions from small packings of spheres. Nature 217, 733–735.
Ogbonna, N., Fleck, N.A., Cocks, A.C.F., 1995. Transient creep analysis of ball indentation. Int. J. Mech. Sci. 37(11), 1179–1202.
Ogden, R.W., 1984. Non-linear Elastic Deformations. Ellis-Horwood, London.
Rice, J.R., 1970. On the structure of stress–strain relations for time-dependent plastic deformation in metals. 37, 728–737.
Shima, S., Oyane, M., 1976. Plasticity theory for porous metals. Int. J. Mech. Sci. 18, 285–291.
Scott, G.D., 1962. Radial distribution of the random close packing of equal spheres. Nature 194, 956–957.
Storåkers, B., 1997. Local contact behaviour of viscoplastic particles. Presented at the IUTAM Symposium on Mechanics of Granular Flow and Powder Compaction, 15–17 July 1996, Cambridge, U.K., ed. N. A. Fleck and A. C. F. Cocks. Kluwer Academic Publishers, pp. 173–184.
Storåkers, B., Larsson, P.-L., 1994. On Brinell and Boussinesq indentation of creeping solids. 42(2), 307–332.
Storåkers, B., Biwa, S., Larsson, P.-L., 1997. Similarity analysis of inelastic contact. International Journal of Solids and Structures 34(24), 3061–3083.
Turner, C.D., Ashby, M.F., 1995a. The cold isostatic pressing of composite powders I. Experimental investigations using model powders, to be published.
Turner, C.D., Ashby, M.F., 1995b. The cold isostatic pressing of composite powders II. Modelling of the initial stage of densification, to be published.
Walton, K., 1987. The effective moduli of random packing of spheres. Journal of the Mechanics and Physics of Solids 35, 213–226.
Wilkinson, D.., Ashby, M. F., 1975. Pressure sintering by power-law creep. Acta Metallurgica 23, 1277–1285.